Published in "Molecular Physics 113(13-14): 1712–1727, 2015"
which should be cited to refer to this work.

On exchange coupling and bonding in the $Gd_2@C_{80}$ and $Gd_2@C_{79}N$ endohedral dimetallo-fullerenes

Fanica Cimpoesu[a], Bogdan Frecus[a], Corneliu I. Oprea[b], Harry Ramanantoanina[c], Werner Urland[c] and Claude Daul[c,*]

[a]*Institute of Physical Chemistry, Bucharest, Romania;* [b]*Department of Physics, Ovidius University of Constanţa, Constanţa, Romania;* [c]*Department of Chemistry, University of Fribourg, Fribourg, Switzerland*

A series of computational experiments performed with various methods belonging to wave-function and density functional theories approaches the issue of bonding regime and exchange coupling in the title compounds. $Gd_2@C_{80}$ is computed with a very weak exchange coupling, the sign depending on the method, while $Gd_2@C_{79}N$ has resulted with a strong coupling and ferromagnetic ground state, irrespective of the computational approach. The multi-configuration calculation and broken symmetry estimation are yielding closely coincident coupling constants, of about $J \sim 400$ cm^{-1}. No experimental estimation exists, but the ferromagnetic ground state of $Gd_2@C_{79}N$ is confirmed from paramagnetic resonance data. The different behaviour is due to particularities of electron accommodation in the orbital scheme. The exchange effects localised on atom lead to preference for parallel alignment of the electrons placed in the 4f and 5d lanthanide shells, determining also a ferromagnetic inter-centre coupling. The structural insight is completed with a ligand field analysis of the density functional theory results in the context of frozen density embedding. The energy decomposition analysis of bonding effects is also discussed. Finally, with the help of home-made codes (named Xatom+Xsphere), a model for the atom encapsulated in a cage is designed, the exemplified numeric experiments showing relevance for the considered endohedral metallo-fullerene issues.

Keywords: lanthanide ions; exchange coupling; endohedral fullerenes; density functional theory; ligand field theory; numeric experiments

1. Introduction

The fullerenes encapsulating [1] atomic or small molecular moieties are objects of interest for the academic insight in bonding regime and also challenging for application perspectives in the line of desiderata for nanoscale technologies [2]. The encapsulated fragments, whose structures are enforced by the cage, are often structures without a standalone identity. In the spirit of structure–property causal relationships, special manifestations are expected for guest–fullerene complexes, originating from the guest or cage sides, or from their particular interaction features. The theoretical accounts are important [3], complementing the experiment with useful explanatory and prediction hints, since such compounds are obtained in very small amounts, often insufficient for full series of instrumental characterisation.

Recently [4] we considered the case of $DySc_2N@C_{80}$ molecule with special behaviour of single ion magnet [5], performing calculations in the frame of density functional theory (DFT) and complete active space self-consistent field (CASSCF), and subsequent modelling using the ligand field (LF) concepts. We illuminated bonding mechanisms, revealing an organo-metallic regime and explained the magnetic anisotropy with the help of an original methodology, drawing the polar surfaces of state-specific magnetisation functions. In the $DySc_2N@C_{80}$ case, we adapted to the metallo-fullerenes procedures of calculation and analysis proven systematically successful in many case studies devoted to the molecular magnetism [6] and optical spectroscopy of lanthanide-based systems [7]. Because of weakly interacting capabilities of active electrons in lanthanides, placed in orbitals with small radial extension, the calculation of lanthanide complexes is not straightforward, a part of the conceptual difficulties being technically manifested as severe convergence problems. The approach implies certain particularised interventions, beyond the usual routine. The authors claim pioneering advances in the computational approach of lanthanide complexes, such as the control of orbital and spin population in DFT calculations [8], revealing the interaction parameters in the frame of the so-called ligand field density functional theory (LFDFT) [9]. In the multi-configuration procedures, an important methodological clue is the initialisation of self-consistent cycles with orbitals merged from corresponding fragments, previously computed separately, namely, the free lanthanide ions and the rest of the molecule [10]. This

* Corresponding author. claude.daul@unifr.ch

starting procedure obeys the physical fact of a canonical space made of almost pure f orbitals, in line with their weak interaction with the environment. The calculation results are optimally exploited when filtered by phenomenological models, the f-type LF approach being a non-trivial issue, transparently operated with the particular modification of the angular overlap model (AOM) [11,12].

With such a basket of methodologies, we attempt the study of lanthanide ion dimers embedded in fullerenes. There are many examples of $Ln_2@C_{78}$, $Ln_2@C_{80}$, $Ln_2@C_{82}$ molecules [13], as well as similar varieties [1]. The extremely stable $La_2@C_{80}$ species, owed to the fact that the C_{80} cage takes all the outer valence electrons of the encapsulated La atoms, was firstly isolated and characterised by the group of Nagase and co-workers [14,15]. The $La_2@C_{78}$ and $Ce_2@C_{78}$ di-metallo-fullerene species with D_{3h} symmetry of the cage were investigated by means of nuclear magnetic resonance (NMR) spectroscopy and X-ray diffraction [16]. Similar methods were used to investigate Er_2 and Tm_2 couples encapsulated in larger C_{82} cage with C_s symmetry [17]. Source of branching out numerous chemical species resides in the isomerism of the cage, as well as in the many orientation conformers of the lanthanide ions with respect of the fullerene skeleton, the energy barriers between the mutation congeners being small.

A point of interest is represented by the interaction enforced between the two ions, 'naked' Ln_2^{6+} systems obviously not existing, because of high charge repeal. The nature of lanthanide–fullerene interaction is another aim of analysis. Though not bonded, the ions of the lanthanide couple should show magnetic interactions whose nature is interesting, in circumstances of enforced mutual encounter. An interesting case, on which we will focus in the following, is the $Gd_2@C_{79}N$ molecule, reported as a ferromagnetic coupling between the two gadolinium ions [18]. The $Gd_2@C_{79}N$ di-metallo-heterofullerene is formally derived from $Gd_2@C_{80}$ with icosahedral symmetry of the cage, a comparison between the two systems being considered.

Figure 1 illustrates the features of lanthanide ions that determine the specifics of weakly interacting f shell, namely, the shrinkage of its radial profile inside the atomic body, below the ionic radius. The f shell itself cannot contribute to the bonding in other manner than the ionic interaction, because of their small radius. In turn, the 5d virtual shell of the lanthanide is accepting the donor activity of the ligands.

In a study dedicated to the situation of quasi-generalised ferromagnetism of the Cu(II)–Gd(III) complexes, evidenced experimentally [19], we performed the first state of the art CASSCF calculations on d–f complexes at realistic scale [10], providing the underlying methodological breakthrough of the merged fragment initialisation of iterative process. The mechanisms were found in line with the qualitative guess, namely, a fraction of the spin from the d-centre arrives, by delocalisation over the ligand bridge, in the 5d orbitals of the lanthanide, conserving the spin polarisation

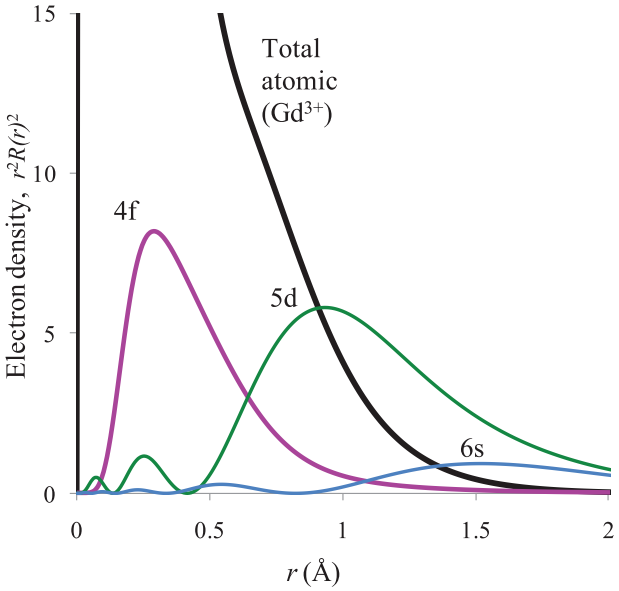

Figure 1. The radial electron density carried by the 4f shell in Gd(III), in comparison to the total atomic density. The 4f shell is shielded from interaction with the chemical environment, while the 5d and 6s virtual shells are able to interact with the neighbourhood, ensuring the bonding of lanthanide ions. The results are obtained with the TZ2P basis set from the ADF code.

along this interaction channel. Given the preference of parallel alignment of the spins on the same atom, the fraction of spin population arrived by weak covalence on the 5d lanthanide shell, effectively aligns in the same way the 4f unpaired electrons. The scheme is, in principle, more general, implying ferromagnetic-type coupling for virtually any d–f bridged interactions, beyond the Cu–Gd case. However, for system other than gadolinium complexes, the orbital moments resulted from quasi-degeneracy of lanthanide-based multiplets and the strong spin–orbit coupling interaction hinder the characterisation in exchange coupling terms. At the same time, the generality of the above mechanism raises the question of prerequisites for the opposed case, of antiferromagnetic involvement of the lanthanide ions. For this issue, we presented relatively recently a case study and a mechanism [6]. Namely, the d–f antiferromagnetism becomes possible when the direct delocalisation of the d-type orbitals carrying the spin is hindered by symmetry reasons (for instance, the d unpaired electron is placed in an orbital with δ overlap features, with respect to a bridge allowing only π-type interaction). Then, if the symmetry-allowed channel is used by a doubly occupied d orbital of the transition metal, it communicates with the 5d virtuals of the lanthanides in a spin-polarised manner. The opposite spin polarity (with respect to the d-type site) is transmitted from the fraction located in the 5d-type orbitals to those of the f shell, by the one-centre exchange forces that drive the preference for aligned one-site spins, the whole succession leading to anti-parallel 3d vs. 4f coupling. The role played

by the 5d orbitals in exchange is possible because of their essential implication in the bonding [20].

The situation of the lanthanide dimers embedded in fullerenes is somewhat different from the regular coordination complexes. The following study clarifies the basic aspects. In the actual numerical experiments, we chose Gd(III) as lanthanide component, in order to focus on the exchange effect, free from magnetic anisotropy effects encountered in other ions.

The bonding regime in metallo-fullerenes without bridging atoms received special attention [21], given the rather intriguing situation of detecting binding effects even in the situation of strong electrostatic repeal between embedded ions. The situation is due to highest occupied molecular carrying bonding features, sometimes combined with a charge transfer from fullerene cage, producing lanthanides in lower oxidation states [22], with metal ion components having the aspect of spd hybrids [23]. However, the bonding mechanisms were not yet completely revealed and a more dedicated attention is expected in the respect of exchange coupling modelling.

To the best of our knowledge, there are no experimental fit of exchange coupling constants, most probably because of the limited sample amounts. The known estimations are due to computation experiments, as is the case of the antiferromagnetic parameter $J = -1.8$ cm^{-1} between Gd(III) ion and the paramagnetic cage, for the Gd@C_{82} mononuclear system [24].

The reported ferromagnetism of the Gd_2@C_{79}N and other structural features were previously sustained [18] with thorough experimental investigations, based on electron paramagnetic resonance. This work [18] also included state of the art DFT calculations but do not advanced toward the computation of the exchange coupling, as the experimental data do not afforded its estimation. We give in the following the complementary account.

2. Calculations

The GAMESS [25] quantum chemistry program was used for the robustness with respect to the CASSCF calculations, employing the SBKJC (Steven–Bash–Krauss–Jensen–Cundari) [26] effective core potential and basis for lanthanide, whereas 6-31G basis set was used for C and N atoms. Previously studied case of $DySc_2N$@C_{80} showed [4] that enhancing the basis on non-metal ions to 6-31G* does not bring significant changes to the results and also the SBKJC performs comparable to full electron basis sets in problems related to magneto-chemistry. The effective core potential was proven a good choice in previous studies of molecular magnetism, leading to a realistic reproduction of experimental data [6,10]. This is due to the reliable account of the f-type orbitals, which matters essentially in such problems. The code ORCA [27] was found particularly convenient for broken-symmetry density functional theory (BS-DFT) calculations, because of the user-friendly spin-flip commands. The Amsterdam density functional (ADF) [28] package is suited for numeric experiments based on controlling the orbital population, having appropriate keywords to impose non-aufbau configurations and fractional occupation numbers. For the ADF calculations, we used TZ2P basis sets (triple zeta with polarisation). In the DFT calculations, performed either with Gaussian-type orbitals (by GAMESS and ORCA) or by Slater-type orbitals (by ADF), we used the BP86 Becke–Perdew functional [29]. The results keep their qualitative sense upon changing the functional, but we avoided to branch out the discussion in this sense, confining to the semi-quantitative respects and the conventionally chosen functional.

3. Results and discussion

3.1. *Exchange coupling of lanthanide dinuclears in fullerenes. Multi-configuration and broken symmetry density functional (BS-DFT) study*

The icosahedral isomer of the C_{80} has a fourfold degenerate highest occupied molecular orbital g_g, occupied with only one pair of electrons [2]. This situation is not convenient for the neutral species, implying instability and distortions. The closed shell structure, $(g_g)^8$, is achieved for the highly negatively charged $C_{80}{}^{6-}$ ion, which then becomes favourable for hosting positive ions, the ensemble being proven as stable. The $C_{79}N$ has the same skeleton as the icosahedral C_{80}, but the symmetry is lowered to C_s point group, having no orbital sets with large degeneracy. However, the trend for acquiring negative charges is kept because of a quasi-degenerate sequence, the closed shell configuration being achieved at the five negative anion, $(C_{79}N)^{5-}$. In Ln_2@C_{79}N compounds, the cage formally charged with six electrons, $(C_{79}N)^{6-}$, carries an unpaired electron. Then, the Ln_2@C_{79}N system can be formally considered as a symmetric trinuclear MXM, with M corresponding to the Gd(III) ions ($S_M = 7/2$) and X the spin originating from the cage, with $S_X = 1/2$. In turn, the Ln_2@C_{80} is, from the magnetic point of view, a genuine dimer, with the fullerene possibly influencing the magnetic orbitals, but not entering in the spin count.

For the Gd_2@C_{80}, the spin Hamiltonian is ascribed in the well-known Heisenberg phenomenology:

$$\hat{H}_{MM} = -2J_{MM}\hat{S}_{M(1)} \cdot \hat{S}_{M(2)}, \tag{1a}$$

with J_{MM} as the inter-lanthanide coupling, the spectrum of states having a simple formula:

$$E_{MM}(S_{MM}) = -J_{MM}S_{MM}(S_{MM}+1), \tag{1b}$$

as function of S_{MM}, the total spin quantum number, ranging from $S_{MM} = 0, 1, \ldots 7$.

For the $Gd_2@C_{79}N$, formulated as trimer, the Hamiltonian is

$$\hat{H}_{MXM} = -2J_{MM}\hat{S}_{M(1)} \cdot \hat{S}_{M(2)} - 2J_{MX}\hat{S}_X \cdot \hat{S}_{M(1)} - 2J_{MX}\hat{S}_X \cdot \hat{S}_{M(2)}, \quad (2a)$$

where J_{MX} is the interaction between Gd(III) body and the orbital carrying the supplementary spin. For symmetric MXM systems, the energies can be expressed analytically by the so-called Kambe formulas:

$$E_{MXM}(S_{MXM}, S_{MM}) = -J_{MX}S_{MXM}(S_{MXM} + 1) + (J_{MX} - J_{MM})S_{MM}(S_{MM} + 1), \quad (2b)$$

where S_{MM} is an intermediate count of the Gd_2 subsystem, and S_{MXM} is the total spin, organised in series with $S_{MXM} = |S_{MM} \pm 1/2|$ parentage. Equations (1b) and (2b) originate from the handling of scalar product operator, eliminating at the end the constant terms.

The most straightforward result is obtained from multi-configurational calculations. Briefly exposed, the CASSCF calculations on $Gd_2@C_{79}N$ revealed a ferromagnetic ground state, with $S = 15/2$ maximal spin, the next gaps, to the respective $S = 13/2$, $11/2$ and $9/2$ states being 407.3, 814.5 and 1220.2 cm^{-1}. One observes the regularity of equal spacing of the energy levels, or, in other words, the approximate 1:2:3 ratio for the presented values. This is in line with the predominance of a large J_{MX} value over a small J_{MM} coupling. More exactly, the outlined states are in line with the following levels: $E_{MXM}(15/2,7) = 0$, $E_{MXM}(13/2,6) = J_{MX} + 14J_{MM}$, $E_{MXM}(11/2,6) = 2J_{MX} + 26J_{MM}$, $E_{MXM}(9/2,6) = 3J_{MX} + 36J_{MM}$, obtained from Equation (2b), after substracting the highest spin as the origin of the energy scale. The presented sequence clearly illustrates the pattern of the exchange, based on a large J_{MX} ferromagnetic coupling, the fitted values being $J_{MX} = 407.11$ cm^{-1} and $J_{MM} = 0.011$ cm^{-1}. Unfortunately, the experimental data do not allow the fit of the coupling parameters, the ferromagnetic nature of the ground state being known only from electron paramagnetic resonance [18].

The calculation on the $Gd_2@C_{80}$, having the regime of the dimer described by the Hamiltonian (1a), yielded $J_{MM} = 0.027$ cm^{-1}, namely, a weak ferromagnetic coupling comparable to those found in the $Gd_2@C_{79}N$ heterofullerene case. The experiment does not provide sufficient magnetic data, the $Gd_2@C_{80}$ species being only transiently characterised [30].

A perspective on the mechanism is gained looking at the canonical orbitals resulted from the CASSCF calculations with 15 electrons in 15 orbitals. For the $Gd_2@C_{79}N$ case, we prepared the starting orbitals merging the f sets of the two Gd(III) ions with the singly occupied molecular orbital (SOMO) of the $(C_{79}N)^{6-}$, computed in preamble as separate units. Actually, the SOMO was obtained as the natural orbital with population close to unity from unrestricted DFT calculations. The f-type orbitals kept their almost pure atomic nature, the calculation bringing only the in-phase and out-of-phase combination in forming orbitals with $a + b$ and $a - b$ respective molecular pattern. However, the orbital initially invested on the cage was changed during the self-consistent-field procedure, ending with a function located on the Gd(III)–Gd(III) moiety. Its orbital composition looks like the in-phase combination of local hybrids with s–d–f content, leading to a bonding-type molecular combination, carrying an unpaired electron. At the same time, examining carefully the shape of the f-type orbital figured on the left-hand side of Figure 2, consisting in the in-phase combination of the z^3 orbitals, one notes a slight asymmetry of the lobes at one centre, suggesting the hybridisation with polar components, s and z^2. This feature can be interpreted as a counterpart of the formation of the canonical orbital represented on the right-hand side,

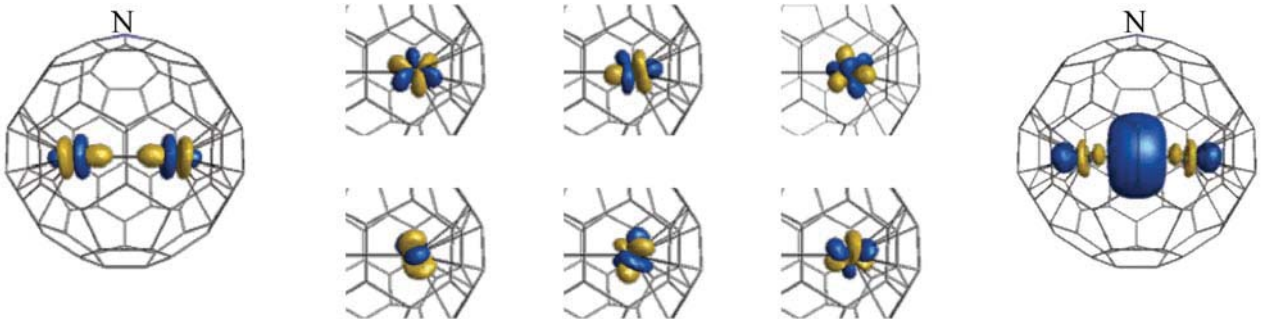

Figure 2. Components of the canonical orbitals from the CASSCF calculation of the $Gd_2@C_{79}N$ system. The orbitals associated with lowest and highest energies are depicted at left-hand and right-hand sides, respectively. The atomic elements shown in the middle panel, only for one site, must be conceived as forming in-phase and out-of-phase combinations with similar functions on the mirror site. The nitrogen atom is figured at the top of the molecule. The system has C_s point group, with the symmetry plane passing through the nitrogen atom and mirroring the lanthanide ions. The isosurfaces are drawn at 0.05 electrons/$Å^3$.

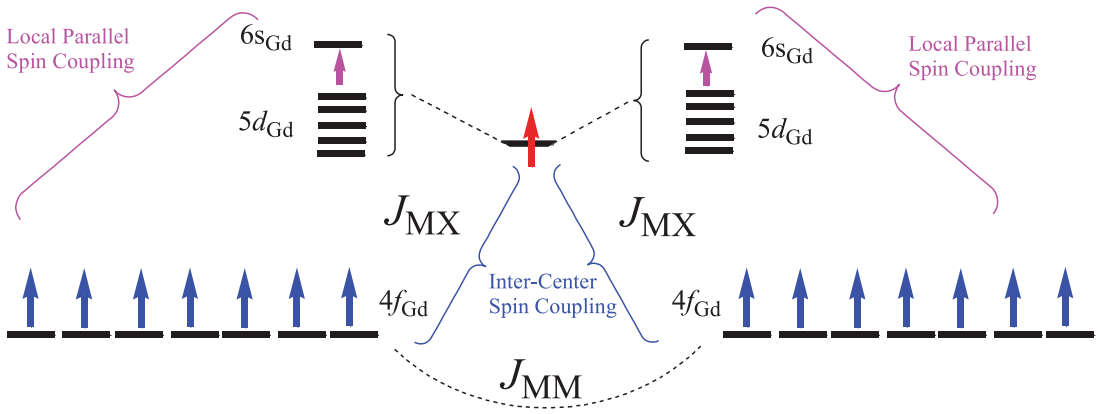

Scheme 1. Mechanism of the ferromagnetic coupling in the $(Gd_2)^{5+}$ dimer in $Gd_2@C_{79}N$.

mainly consisting in z^2 and s components, with z^3-type traces. Though having lower canonical energies, the f-type orbitals of the CASSCF run are non-bonding type, as compared to the upper one, having bonding pattern. One has to point out that the orbital energies of canonical sets do not have solid physical meaning, being merely objects to construct the multi-configuration problem. Their alteration by unitary transformation does not change the eigenvalues. The discussion in terms of orbital energies has therefore qualitative purpose. For instance, the mentioned upper orbital has a higher canonical energy because it is made of 5d and 6s atomic orbitals, placed above the 4f set in atomic schemes.

The interaction pattern is represented in simplified manner in Scheme 1. The electron located in the orbital with upper canonical energy (right-hand side of Figure 1) practically corresponds to the X centre discussed in the spin Hamiltonian. This function took the place initially assigned to the SOMO of the $(C_{79}N)^{6-}$ cage. In the Gd(II) ion, with $(4f)^7(5d)^1$ configuration, the f and d electrons will prefer parallel alignment. The formation of SOMO bonding-type upper canonical orbital implies a mixed-valence-alike situation, the gadolinium site being projected in a Gd(III) + Gd(II) superposition. The 5d-type fraction of one-half of electron assigned to each Gd(III) core aligns its spin to those of seven parallel unpaired electrons from the f shell. This effect makes the electron placed in the upper 5d-type bonding molecular orbital to look ferromagnetically coupled with both lanthanide sites. In other words, formally, the f spin from one centre is forced to be parallel with the d-type one, when it is placed on the other lanthanide site. Apparently, in this description, the hetero-fullerene plays a little role, just hosting the artificial dinuclear. However, if we draw the canonical orbitals at lower density contours, the tails located on the cage become visible, so that the fullerene participates in a spin polarisation mechanism.

In the following, we will switch the analysis tools, meeting the terms of BS-DFT [31]. As well known, the DFT is a single determinant method, while the magnetic states are, in general, multi-configuration objects. Although, the DFT can approach the molecular magnetism by appropriate numeric experiments, the BS states having not a physical reality, but being appropriately tailored to reveal information on the spin Hamiltonian parameters. In the crudest approximation, the BS states are interpretable with the Ising-type Hamiltonian, replacing the scalar product of spin operators with numeric multiplication of the local spin projections, $S_{z(A)}S_{z(B)}$. The Ising terms are actually the diagonal of a full Heisenberg Hamiltonian. In the BS phenomenology, the total switch of the spin at one centre implies that only the $+S_AS_B$ or $-S_AS_B$ (positive or negative) amounts are allowed. The Ising interpretation would be valid if the BS calculation will be based on restricted-type orbitals, with the same space contours for corresponding α and β sets. However, the BS calculations are conceived and carried out in unrestricted spin schemes. In such circumstances, one may conceive the $|\hat{S}_A \cdot \hat{S}_B|$expectation value as parameter $|\langle \hat{S}_A \cdot \hat{S}_B \rangle|$ entering with plus or minus signs, $\pm|\hat{S}_A \cdot \hat{S}_B|$, in the formulation of the expectation value of the spin Hamiltonian, if the given configuration records, respectively, identical or opposite spin polarities on the A and B centres. For the MXM trimer formulation of the di-lanthanido-heterofullerene case, there are three distinct BS configurations: $\Omega(HS) = M(1)^+X^+M(2)^+$, $\Omega(BS1) = M(1)^+X^-M(2)^+$ and $\Omega(BS2) = M(1)^+ X^+M(2)^-$. The first one corresponds to high spin (HS) ferromagnetic alignment of all the spin densities, computed at maximal spin projection, $S_z = 15/2$. The expectation value from a BS configuration Ω of the Hamiltonian in Equation (2a) is ascribed as follows:

$$\begin{aligned}\langle\Omega|\,\hat{H}_{MXM}\,|\Omega\rangle = E_0 &- 2\sigma^{\Omega}_{M(1)}\sigma^{\Omega}_{M(2)}J_{MM}\left|\langle\hat{S}_{M(1)}\cdot\hat{S}_{M(2)}\rangle\right| \\ &- 2\sigma^{\Omega}_{X}\sigma^{\Omega}_{M(1)}J_{MX}\left|\langle\hat{S}_{X}\cdot\hat{S}_{M}\rangle\right| \\ &- 2\sigma^{\Omega}_{X}\sigma^{\Omega}_{M(2)}J_{MX}\left|\langle\hat{S}_{X}\cdot\hat{S}_{M}\rangle\right|, \qquad (3)\end{aligned}$$

where the σ coefficients are ± 1 factors with respect to spin up or spin down population of the given centre, in the considered configuration. In the HS configuration, we have all the coefficients equal to unity: $\sigma^{HS}_{M(1)} = 1$, $\sigma^{HS}_{X} = 1$, $\sigma^{HS}_{M(2)} = 1$. For the BS1 configuration, the spin on the X subsystem is flipped, having therefore: $\sigma^{BS1}_{M(1)} = 1$, $\sigma^{BS1}_{X} = -1$, $\sigma^{BS1}_{M(2)} = 1$. The BS2 case flips the spin on the second metal ion: $\sigma^{BS2}_{M(1)} = 1$, $\sigma^{BS2}_{X} = 1$, $\sigma^{BS2}_{M(2)} = -1$. The E_0 energy shift was made explicit in Equation (3) in order to formally account an absolute value. However, it is sufficient to consider the relative differences, for instance, with respect to the HS configuration. In this case, the relative BS state energies of the trimer are

$$\Delta E_{BS1} = E_{BS1} - E_{HS} = 8 J_{MX} |\langle \hat{S}_X \cdot \hat{S}_M \rangle|, \tag{4a}$$

$$\Delta E_{BS2} = E_{BS2} - E_{HS} = 4 J_{MM} \left|\left\langle \hat{S}_{M(1)} \cdot \hat{S}_{M(2)} \right\rangle\right| + 4 J_{MX} |\langle \hat{S}_X \cdot \hat{S}_M \rangle|. \tag{4b}$$

The expectation values of the squared spin operator can also be equated with the $|\hat{S}_A \cdot \hat{S}_B|$ parameters:

$$\langle \Omega | \hat{S}^2 | \Omega \rangle = ct + 2\sigma^{\Omega}_{M(1)}\sigma^{\Omega}_{M(2)} \left|\left\langle \hat{S}_{M(1)} \cdot \hat{S}_{M(2)} \right\rangle\right| + 2\sigma^{\Omega}_{X}\sigma^{\Omega}_{M(1)} |\langle \hat{S}_X \cdot \hat{S}_M \rangle| + 2\sigma^{\Omega}_{X}\sigma^{\Omega}_{M(2)} |\langle \hat{S}_X \cdot \hat{S}_M \rangle|. \tag{5}$$

The constant term is, in the case of the considered trimer, $ct = 2S_M(S_M + 1) + S_X(S_X + 1)$, where $S_M = 7/2$ and $S_X = 1/2$, estimating $ct = 129/4 = 32.25$. In similitude to the energy treatment, the relative differences to the HS configuration can be considered:

$$\Delta \langle S^2 \rangle_{BS1} = -8 |\langle \hat{S}_X \cdot \hat{S}_M \rangle|, \tag{6a}$$

$$\Delta \langle S^2 \rangle_{BS2} = -4 |\langle \hat{S}_{M(1)} \cdot \hat{S}_{M(2)} \rangle| - 4 |\langle \hat{S}_X \cdot \hat{S}_M \rangle|. \tag{6b}$$

The BS-DFT treatment (with BP86 functional and the previously mentioned basis sets) gives the following energy gaps: $\Delta E_{BS1} = 6113.24$ cm^{-1} and $\Delta E_{BS2} = 1927.64$ cm^{-1}. The unrestricted DFT calculation prints out the expectation values for the$\langle S^2 \rangle$, which for the HS, BS1 and BS2 cases are 63.82, 49.79 and 7.8, respectively. Differences of -14.93 and -56.33 correspond to Equations (6a) and (6b). These relative values determine the parameters $|\langle \hat{S}_X \cdot \hat{S}_M \rangle| = |\langle \hat{S}_X \cdot \hat{S}_M \rangle| = 1.87$ and $|\langle \hat{S}_{M(1)} \cdot \hat{S}_{M(2)} \rangle| = |\langle \hat{S}_{M(1)} \cdot \hat{S}_{M(2)} \rangle| = 12.22$, quite close to the simplistic Ising-type limits, $S_X S_M = (1/2)(7/2) = 1.75$ and $S_M S_M = (7/2)(7/2) = 12.25$, respectively. The fitted parameters account also for the absolute computed $\langle S^2 \rangle$ amounts, when replaced in Equation (5) altogether with the ideal $ct = 32.25$ shift. The overall fit of formulas (4) and (6) to the values outlined from the BS computations yields the exchange coupling parameters: $J_{MX} = 409.60$ cm^{-1} and $J_{MM} = -23.11$ cm^{-1}. One notes the remarkable closeness of J_{MX} value to those computed in the CASSCF treatment. In turn, J_{MM} is negative and possibly slightly overestimated. This discrepancy does not affect the qualitative and semi-quantitative picture, common to both approaches, namely, a dominating ferromagnetic MX type of coupling, overriding the direct MM interaction, irrespective of its ferromagnetic or antiferromagnetic nature. Figure 3 shows the spin density maps of the discussed calculations, confirming the BS nature of the configurations BS1 and BS2. The role of the fullerene cage, involved in a spin polarisation effect, is illustrated by visible density tails.

The BS-DFT treatment of the $Gd_2@C_{80}$ leads to a small antiferromagnetic exchange coupling $J_{MM} = -2.66$ cm^{-1}. It is opposite to the CASSCF result, but clearly testifies the small intensity of the interaction, if compared to the spin active cage of the mono-nitrogen hetero-fullerene.

As noted in the technical section, the BS calculations were easily done with the ORCA program [27], that has an explicit keyword for switching the local spins with respect to an HS reference, computed in preamble. Without this facility, the series of BS calculations can be achieved by operations of orbital localisation and subsequent permutations between and inside α and β subsets, preparing educated guesses, aimed to prefigure the desired spin polarisation scheme. However, the success of BS calculations is not always guaranteed, being dependent also on some uncontrolled tacit factors, such as the anatomy of the basis sets or the canonicalisation scheme of the molecular orbitals. The ADF suite [28] also has a spin flip facility. However, we were not able to obtain in ADF results similar to those performed by ORCA, for $Gd_2C_{79}N$. With ADF, we catch only the HS and BS1 configurations which show a gap of 3216.6 cm^{-1} and a difference of about -14.02 (Equation (6a)) in the expectation value of the squared spin. This allows the estimation of $J_{MX} = 229.5$ cm^{-1}, which is smaller than those found in the previous BS treatment, but yet preserves the range of strong ferromagnetic coupling. One has to point out that the BS1 configuration was obtained by ADF in non-aufbau conditions, having the β spin assigned to the X orbital component placed above the 14 empty f-type β orbitals. This scheme seems to keep, inside the β virtuals, the atomic pattern with 5d and 6s above the 4f levels originating from the two ionic bodies. This structure possibly appears due the use of Slater-type orbitals and its technical realisation is due to the ADF capability in dealing with non-aufbau situations. The partial success of the ADF in the BS account of exchange effect is reflected in a spurious mixing of the f-type orbitals with the fullerene components, obtaining a net polarisation of about 6.4 α spin on this shell, while the ORCA approach gives the α net population of 6.95, closer to the idea of weakly interacting f atomic orbitals.

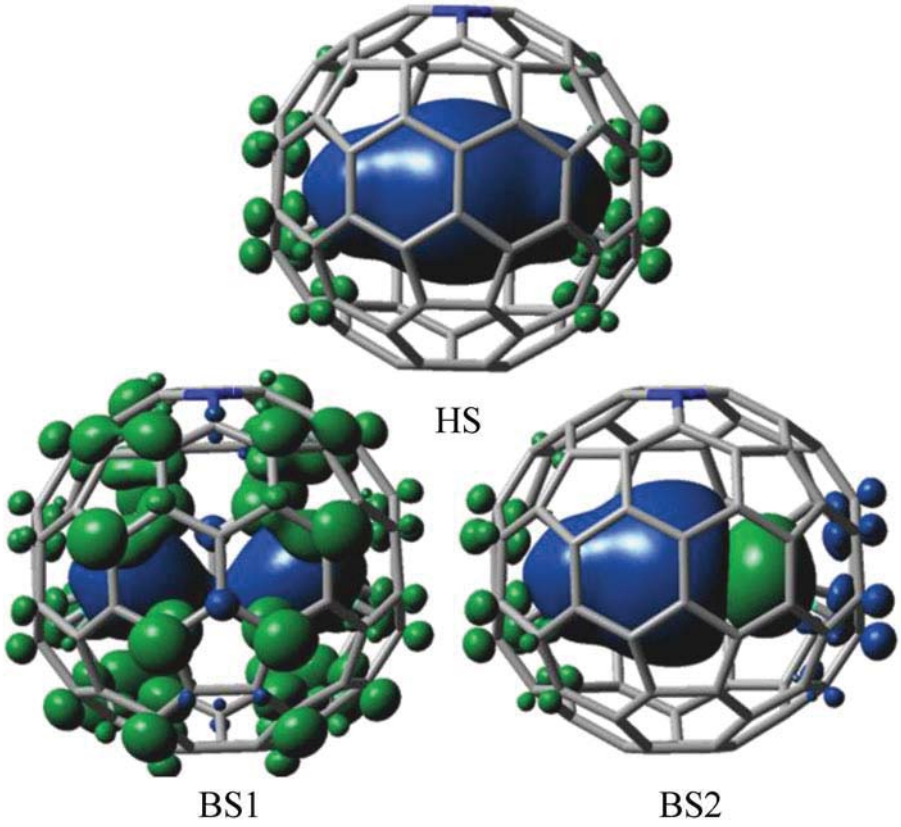

Figure 3. Spin density maps for the configurations related to the BS-DFT estimation of exchange parameters. The dark surfaces correspond to α spin density and while light tones to β spin. The high spin state HS (up) and the broken symmetry states BS1 and BS2 (down) correspond, respectively, to the $M(1)^+X^+M(2)^+$, $M(1)^+X^-M(2)^+$ and $M(1)^+X^+M(2)^-$ spin polarisations. The isosurfaces are drawn at 0.05 electrons/Å^3.

Employing other special feature of the ADF, we performed BS calculations under the conditions of the so-called frozen density embedding (FDE) [32]. This technique is a reasonable approximate account of the subsystems with a relatively small hybridisation with a certain environment, as expected for the f shell of lanthanides. The $(C_{79}N)^{5-}$ diamagnetic negative cage was defined as frozen subsystem, with the mixed valence $(Gd_2)^{5+}$ moiety as guest. The dimer HS state has a configuration ascribed as $[Xe]_2(\sigma_f)^\alpha(\sigma_f{}^*)^\alpha\ (\pi_f)^{2\alpha}(\pi_f{}^*)^{2\alpha}(\delta_f)^{2\alpha}(\delta_f{}^*)^{2\alpha}(\varphi_f)^{2\alpha}(\varphi_f{}^*)^{2\alpha}(\sigma_{d,s})^\alpha$, while the BS1 case has the last orbital switched to the $(\sigma_{d,s})^\beta$ opposite spin. The BS2 configuration was successfully produced by reverting the *f* spins at one lanthanide centre. The orbital system is much similar to those resulted in the CASSCF procedure. The fit of the FDE-BS-DFT results of $(Gd_2)^{5+}$ embedded in the frozen density of the $(C_{79}N)^{5-}$ yielded $J_{MX} = 446.23$ cm^{-1} and $J_{MM} = -2.03$ cm^{-1}. The first coupling parameter is close to those resulted in CASSCF and BS calculations with Gaussian basis sets. The J_{MM} is between the CASSCF and first discussed BS-DFT results. We cannot decide now whether there is a weak ferro or antiferro coupling between the Gd ions, as neither can the experiments enter in such a detail. Giving the credits to DFT, as better descriptor of dynamic correlation effects, the real case is probably a weak antiferromagnetism which, however, cannot be discriminated on the background of the strong ferromagnetic interaction channels.

3.2. Ligand field modelling and frozen density embedding density functional theory calculations

The frozen density embedding (FDE) [32] will be used to figure out the LF regime, because this computation method constructs a perturbation in the sense of such phenomenology. The results are illustrated by the Kohn–Sham orbitals in Figure 4. The qualitative representation of the fullerene proximity altogether with neighbour ion perturbations exerted on a lanthanide site is given in Scheme 2. The Gd–Gd axis points approximately towards the middle of a couple of hexagonal faces of the fullerene cage. The nitrogen atom of the $C_{79}N$ skeleton is distant from the carbon atoms forming the vicinity of the lanthanide ions. Therefore, from the viewpoint of the fullerene-determined perturbation, the local frame follows a six-order pseudo-symmetry axis. This

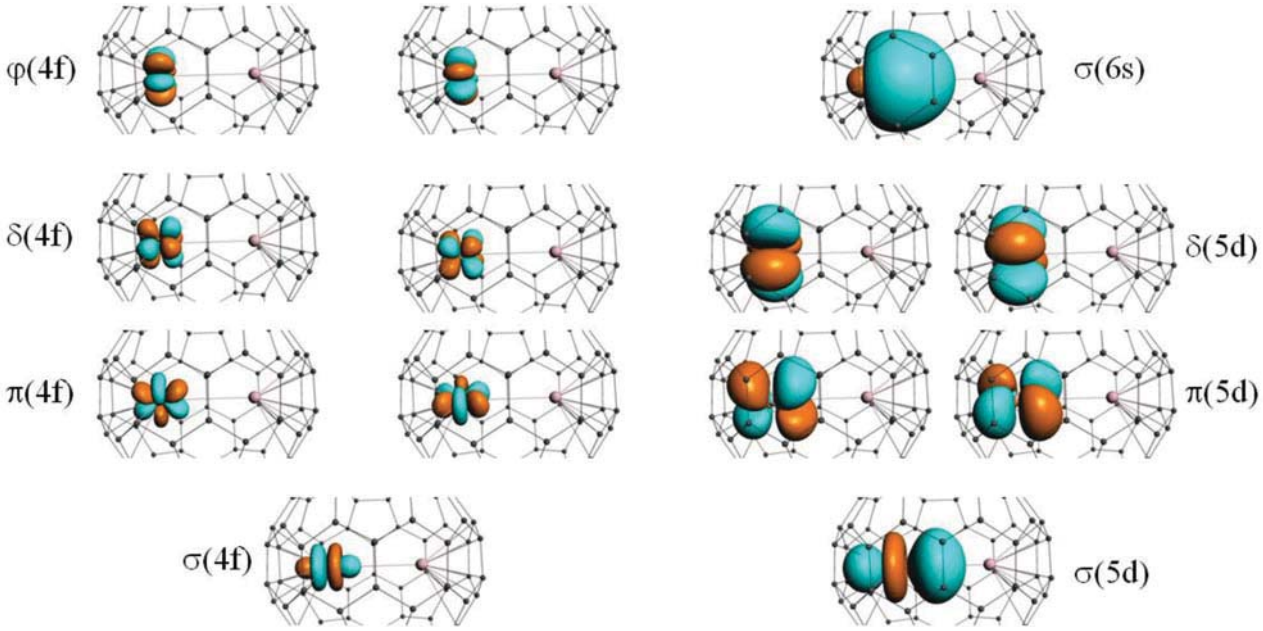

Figure 4. Orbitals from FDE calculation of one Gd(III) centre, considering the other lanthanide site and the fullerene cage as environment. Both the fullerene and the neighbour lanthanide ion exert a perturbation with quasi-linear symmetry to the orbitals originating from 4f, 5d and 6s shells, closely obeying a classification in σ, π, δ, φ labels. The isosurfaces are drawn at 0.04 electrons/Å^3.

also can be interpreted as a quasi-linear symmetry, $C_{\infty v}$, combined with the true linear symmetry, due to the companion lanthanide ion. Formally, the perturbed orbitals can be interpreted as A–Ln–B linear system, the proximal hexagonal face of the fullerene and the point charge of the other metal ion playing the ligand A and B, respectively. However, the energy order is reverted with respect to the customary conception of the LF from linearly ligating ligands. In usual LF [33,34], the σ-type orbitals (z^3 for the f set, or z^2 for the d ones) are most perturbed, because they ensure, in terms of covalence, the strongest metal–ligand overlap. In electrostatic terms, the electron located in f_{z3} or d_{z2} orbitals are closer to the cloud of negatively charged ligand, undergoing the highest destabilisation by Coulomb repulsion. Let us denote the perturbation in the style of the AOM, the e_λ (with $\lambda = \sigma, \pi, \delta, \varphi$) being the energy shifts of the metal-based orbitals in an M–L isolated couple, relative to the free metal ion. The customary order of perturbation is $e_\sigma > e_\pi > e_\delta > e_\varphi$, often assuming $e_\delta \sim 0$ and $e_\varphi \sim 0$, since the ligand orbitals do not span such symmetries. Taking the hexagonal face of fullerene as ligand A, we obtain $e_\varphi{}^{(A)} > e_\delta{}^{(A)} > e_\pi{}^{(A)} > e_\sigma{}^{(A)}$. The z^3 or z^2 lobes are pointing towards the void of the frame, being less perturbed, while orbitals of φ type, with six lobes, intercept in optimal manner the perturbation of the proximal hexagon. Now considering the opposed axis, one may say that the neighbour lanthanide ion is in fact an 'anti-ligand', having positive charge, in opposition to the normal case of negatively charged ligands. Then, taking it as 'ligand B', it also determines reversed perturbation scheme, $e_\varphi{}^{(B)} > e_\delta{}^{(B)} > e_\pi{}^{(B)} > e_\sigma{}^{(B)}$, because of the positive charge. In fact, the B 'anti-ligand' exerts a stabilisation of the electron placed in the f or d shells (negative shift) in contrast to the usual destabilisation due to negatively charged ligands. By different mechanism, the A and B contributions are aligned to give the same ordering of the $\lambda = \sigma, \pi, \delta, \varphi$ states in the quasi-axial symmetry and a common series parameters can be ascribed for their combined action $e_\lambda = e_\lambda{}^{(A)} + e_\lambda{}^{(B)}$. In the given model, one cannot discriminate the individual $e_\lambda{}^{(A)}$ and $e_\lambda{}^{(B)}$, but only their e_λ sums, ordered like

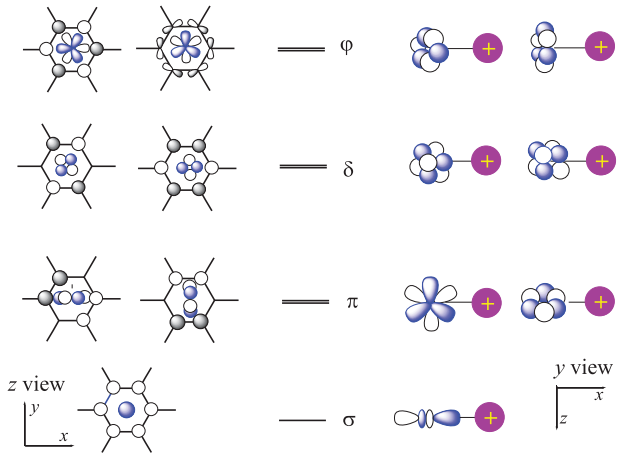

Scheme 2. Ligand Field effects on a lanthanide ion, exerted by a hexagonal frame of the fullerene wall (left side) and the neighbour positive ion (right side), in $Gd_2@C_{80}$ and $Gd_2@C_{79}N$.

$e_\varphi > e_\delta > e_\pi > e_\sigma$. We tacitly discussed in the above part the case of f systems. The situation is, in principle, the same for the d case, after removing from discussion the φ component, non-existent in this set.

The ligand field theories are consecrated for a single-shell case, either d type for transition metal complexes [33] or f-type for lanthanide systems [34]. In each situation, the description is tacitly affected by the so-called holohedrisation [35] effect. Namely, irrespective to the even or odd inversion parity of a given orbital set (e.g. with g label for d and u symmetry for f, respectively), the d–d and f–f Hamiltonian blocks will account only symmetric, g-type, perturbation because of the obvious reason of $g \times g = g$, $u \times u = g$ multiplication rules. This drawback is usually not considered, because in many cases, the coordination chemistry and LF analysis concern relatively symmetric systems, e.g. often octahedral frames, where the caveat is not acting, or is not severe. The artificial effect of holohedrisation can be encompassed designing an extended LF scheme with both odd and even basis components insofar as the off-diagonal block includes the $g \times u = u$ asymmetric components. We recently presented a two-shell extended LF model based on d and f orbitals [36], which needs to be called for the account of the presented case. Indeed, we face a rather visible polarisation of the electrostatic potential, with fullerene as a negatively charged A ligand and the companion metal ion as a positive charge B, acting reversely to the usual ligands.

The orbitals from the FDE-DFT calculation show the discussed ordering in both 4f and 5d sets. Besides, we included an orbital labelled 6s which results actually as a hybrid s–d–f shape. In the following, we will take the orbital energies as approximation for the LF modelling. In general, the orbital energies are not best objects for this purpose. Thus, in a restricted scheme, the double, single or empty functions assignable to the ground-state configuration are subject of different canonicalisation schemes. This leads to different types of two-electron effective interaction that obscures the one-electron potential corresponding to the LF. At the same time, using unrestricted orbitals, thus obtaining different sets of orbitals and energies for the d- or f-type orbitals, is not in line with current principles of the LF theories, demanding an unique form of the d- or f-related molecular functions. Such gaps between the DFT calculations and the attempts of LF modelling can be bridged by the average of configuration (AOC) [8] step enabling the LFDFT subsequent analysis. Aiming for the description of a complex with d^n or f^n configuration, the AOC approach implies the selection of the orbitals with proper d or f parentage, imposing on each of the five or seven components $n/5$ or $n/7$ fractional occupations, respectively. This computational setting gives an average tacitly assumed in LF theory as pseudo-spherical reference. The full LFDFT procedure [8,9] implies then running several artificial configurations, mimicking the many-determinant situations, providing state energies from where the LF parameters can be extracted. This does not mean that DFT itself has become multi-configurational, but, in a manner somewhat similar to BS, it is possible to design states representing numeric experiments containing parameters appropriate for a defined goal, the LF frame, in the LFDFT case. One has to point out that the work with fractional populations [37] is allowed in the conceptual DFT and technically possible with the employed ADF suite [28].

However, using the FDE frame [32], the full numeric experiments of the LFDFT cannot be produced, confining ourselves to the use of orbital energies. Particularly, because of half-filled nature of the f^7 configuration of Gd(III), the resulted orbitals are in fact well tempered for LF considerations, having already the AOC regime.

In the given circumstance, the orbital energies seem a reasonable surrogate for the LF-type ordering. The orbital energies (in electron-volt unit) are grouped in a series corresponding to 4f shell, $\{-27.576, -27.559, -27.556, -27.518, -27.516, -27.464, -27.461\}$ spaced by a large gap from the 5d-type solutions, $\{-17.302, -16.399, -16.37, -15.976, -15.965\}$, which are relatively close to the eigenvalue assignable to the 6s, at -14.742 eV. These results are submitted to the analysis in terms of LF parameters.

The multi-shell LF Hamiltonian can be in this case of axial symmetry confined to the expansion in $Y_{k,0}$ spherical harmonic functions. The diagonal f and d blocks are expressed in standard manner, defining separate sets of parameters, B_0^k (ff) and B_0^k (dd), respectively:

$$\hat{H}_{\mathrm{LF}}^{\mathrm{ff}} = \sum_{k=0,2,4,6} \sqrt{\frac{4\pi}{2k+1}} B_0^k(\mathrm{ff}) Y_{k,0}, \tag{7a}$$

$$\hat{H}_{\mathrm{LF}}^{\mathrm{dd}} = \sum_{k=0,2,4} \sqrt{\frac{4\pi}{2k+1}} B_0^k(\mathrm{dd}) Y_{k,0}. \tag{7b}$$

Note that the above expansions involve only even spherical harmonics sets: $k = 0, 2, 4, 6$ for the Hamiltonian dedicated to the f block, and $k = 0, 2, 4$ for the d one. In usual LF models, dedicated to a single shell, the $k = 0$ terms are not expressed, implying an arbitrary shift, but here we made them explicit, since B_0^0 (dd) $- B_0^0$ (ff) marks the gap between the lower 4f and upper 5d shells. Actually, in this circumstance, the relative difference is not an entirely LF potential element, including the f–d gap, as intrinsic feature of the ion to which LF shifts are added. The odd components ($k = 1, 3, 5$) are appearing in the f–d diagonal block that carries the modelling beyond the holohedrisation limits [36]:

$$\hat{H}_{\mathrm{LF}}^{\mathrm{fd}} = \sum_{k=1,3,5} \sqrt{\frac{4\pi}{2k+1}} B_0^k(\mathrm{fd}) Y_{k,0}. \tag{7c}$$

Once the orbital component originating from the 6s virtual of lanthanide ion, close to the 5d orbitals, is included, one also has the non-diagonal Hamiltonian elements expressing the d–s and f–s mixing terms:

$$\hat{H}_{\mathrm{LF}}^{\mathrm{ds}} = \sqrt{\frac{4\pi}{5}} B_0^2(\mathrm{ds}), \tag{7d}$$

$$\hat{H}_{\mathrm{LF}}^{\mathrm{fs}} = \sqrt{\frac{4\pi}{7}} B_0^3(\mathrm{fs}). \tag{7e}$$

The whole Hamiltonian matrix is sparse, having non-diagonal elements only between the components with the same λ axial symmetry in different shells. Therefore, the σ-type block involves the f, d and s orbitals. Defined in the AOM style, one infers different e_σ parameters for the distinct blocks:

$$h_{\mathrm{LF}}^{\sigma} = \begin{pmatrix} e_\sigma^{\mathrm{ff}} & e_\sigma^{\mathrm{fd}} & e_\sigma^{\mathrm{fs}} \\ e_\sigma^{\mathrm{fd}} & e_\sigma^{\mathrm{dd}} & e_\sigma^{\mathrm{ds}} \\ e_\sigma^{\mathrm{fs}} & e_\sigma^{\mathrm{ds}} & e_\sigma^{\mathrm{ss}} \end{pmatrix}, \tag{8}$$

the matrix elements being defined with respect to the series of Equations (7):

$$e_\sigma^{\mathrm{ff}} = B_0^0(\mathrm{ff}) + \frac{4}{15} B_0^2(\mathrm{ff}) + \frac{2}{11} B_0^4(\mathrm{ff}) + \frac{100}{429} B_0^6(\mathrm{ff}), \tag{9a}$$

$$e_\sigma^{\mathrm{dd}} = B_0^0(\mathrm{dd}) + \frac{2}{7} B_0^2(\mathrm{dd}) + \frac{2}{7} B_0^4(\mathrm{dd}), \tag{9b}$$

$$e_\sigma^{\mathrm{ss}} = B_0^0(\mathrm{ss}), \tag{9c}$$

$$e_\sigma^{\mathrm{fd}} = \frac{3}{\sqrt{35}} B_0^1(\mathrm{fd}) + \frac{4}{3\sqrt{35}} B_0^3(\mathrm{fd}) + \frac{10}{33}\sqrt{\frac{5}{7}} B_0^5(\mathrm{fd}), \tag{9d}$$

$$e_\sigma^{\mathrm{fs}} = \frac{1}{\sqrt{7}} B_0^3(\mathrm{fs}), \tag{9e}$$

$$e_\sigma^{\mathrm{ds}} = \frac{1}{\sqrt{5}} B_0^2(\mathrm{ds}). \tag{9f}$$

The matrix blocks dedicated to the π effects are

$$h_{\mathrm{LF}}^{\pi} = \begin{pmatrix} e_\pi^{\mathrm{ff}} & e_\pi^{\mathrm{fd}} \\ e_\pi^{\mathrm{fd}} & e_\pi^{\mathrm{dd}} \end{pmatrix}, \tag{10}$$

with the following expansions:

$$e_\pi^{\mathrm{ff}} = B_0^0(\mathrm{ff}) + \frac{1}{5} B_0^2(\mathrm{ff}) + \frac{1}{33} B_0^4(\mathrm{ff}) - \frac{25}{143} B_0^6(\mathrm{ff}), \tag{11a}$$

$$e_\pi^{\mathrm{dd}} = B_0^0(\mathrm{dd}) + \frac{1}{7} B_0^2(\mathrm{dd}) - \frac{4}{21} B_0^4(\mathrm{dd}), \tag{11b}$$

$$e_\pi^{\mathrm{fd}} = \frac{5}{\sqrt{70}} B_0^1(\mathrm{fd}) + \frac{2}{3\sqrt{70}} B_0^3(\mathrm{fd}) - \frac{5}{33}\sqrt{\frac{10}{7}} B_0^5(\mathrm{fd}). \tag{11c}$$

The δ-type blocks are also 2 × 2 matrices:

$$h_{\mathrm{LF}}^{\delta} = \begin{pmatrix} e_\delta^{\mathrm{ff}} & e_\delta^{\mathrm{fd}} \\ e_\delta^{\mathrm{fd}} & e_\delta^{\mathrm{dd}} \end{pmatrix}, \tag{12}$$

with the following elements:

$$e_\delta^{\mathrm{ff}} = B_0^0(\mathrm{ff}) - \frac{7}{33} B_0^2(\mathrm{ff}) + \frac{10}{143} B_0^6(\mathrm{ff}), \tag{13a}$$

$$e_\delta^{\mathrm{dd}} = B_0^0(\mathrm{dd}) - \frac{2}{7} B_0^2(\mathrm{dd}) + \frac{1}{21} B_0^4(\mathrm{dd}), \tag{13b}$$

$$e_\delta^{\mathrm{fd}} = \frac{1}{\sqrt{7}} B_0^1(\mathrm{fd}) - \frac{2}{3\sqrt{7}} B_0^3(\mathrm{fd}) + \frac{5}{33\sqrt{7}} B_0^5(\mathrm{fd}). \tag{13c}$$

Finally, the φ components are matrix elements belonging to the f shell only

$$h_{\mathrm{LF}}^{\varphi} \equiv e_\varphi^{\mathrm{ff}} = B_0^0(\mathrm{ff}) - \frac{1}{3} B_0^2(\mathrm{ff}) + \frac{1}{11} B_0^4(\mathrm{ff}) - \frac{5}{429} B_0^6(\mathrm{ff}). \tag{14}$$

Considering the fit by LF modelling, we take the above-mentioned orbital energies, relative to the lowest value, expressed in wavenumber units: $\varepsilon(4\mathrm{f}) = \{0,\ 137.1,\ 161.3,\ 467.8,\ 484.0,\ 903.4,\ 927.6\}\ \mathrm{cm}^{-1}$, $\varepsilon(5\mathrm{d}) = \{82870.1,\ 90153.7,\ 90387.6,\ 93565.6,\ 93654.3\}\ \mathrm{cm}^{-1}$ and $\varepsilon(6\mathrm{s}) = 103519.0\ \mathrm{cm}^{-1}$. For the f suite, is observed a non-degenerate lowest level, followed by quasi-degenerate couples related to the discussed $\sigma < \pi < \delta < \varphi$ ordering. The similar $\sigma < \pi < \delta$ regularity is observed also for the d set. Relative to the lowest d-type level, the energies of the set are 0, 7283.6, 7517.5, 10695.5 and 10784.2 cm^{-1}. One notes the magnitude of the spacing, in the range of hundreds reciprocal centimetres for the f set, while a total gap of about 10,000 wavenumbers for the LF split of d shell, in concordance with general expectation for f and d LF cases [33,34]. The energy ordering can be also corroborated with the down-to-up depiction of the orbital shapes in Figure 4. Observing the slight asymmetry of the orbital lobes, lesser for the f ones and more pronounced for the d cases, one might understand the need for an extended multi-shell LF modelling, as sketched here.

With the corresponding eigenvectors, the eigenvalues are back-transformed to a matrix taking in effectively pure atomic orbital basis of f, d and s shells, as defined in the previous LF modelling. In the process, the diagonal and

Table 1. The ligand field parameters fitting the FDE calculations representing one Gd(III) site in $Gd_2@C_{79}N$ (while the other lanthanide ion and the fullerene cage are taken as frozen density fragments). All values are in cm^{-1}.

(ab)	(ff)	(dd)	(ss)	(fd)	(fs)	(ds)
$B_0^0(ab)$	454.8	91,008.6	99,006.0	0.0	0.0	0.0
$B_0^1(ab)$	0.0	0.0	0.0	2937.1	0.0	0.0
$B_0^2(ab)$	−1420.9	−4578.2	0.0	0.0	0	−19,096.9
$B_0^3(ab)$	0.0	0.0	0.0	853.7	1401.0	0
$B_0^4(ab)$	−156.6	−8240.9	0.0	0.0	0.0	0.0
$B_0^5(ab)$	0.0	0.0	0.0	−82.2	0.0	0.0
$B_0^6(ab)$	−46.2	0.0	0.0	−82.2	0.0	0.0

non-diagonal matrix elements related to the almost equivalent terms, inside double degeneracy of π, δ and φ levels, were averaged. Their deviation with respect to the average was comprised within 0.5%–4%, quite close to the assumed effective symmetry. Then, one may fit the LF parameters to the computed matrix, obtaining the values outlined in Table 1. The $B_0^0(ab)$ values for the different shell (ab) couples can be arbitrarily shifted, all with the same value. The actual set puts in zero of the energy scale the lowest eigenvalue of the whole Hamiltonian. An alternative convention, with $B_0^0(\mathrm{ff}) = 0$ would render $B_0^0(\mathrm{dd}) = 90553.8\ cm^{-1}$ and $B_0^0(\mathrm{ss}) = 98551.2\ cm^{-1}$. One may observe that the fd shell couple holds the odd LF parameters with $k = 1, 3, 5$, while the other parameters span the even inversion symmetry. The approximations included in the FDE approach are in line with the LF concepts, allowing a semi-quantitative insight in the LF regime.

3.3. *Energy decomposition analysis of bonding effects in endohedral metallo-fullerenes*

In the following, we will examine the bonding regime of the lanthanide embedded in fullerene, switching the focus on the $Gd_2@C_{80}$ system. We benefit from the energy decomposition analysis (EDA) implemented in ADF in accordance to Ziegler-Rauk scheme [38]. The total bonding energy is evaluated relative to previously prepared fragments and dichotomised in Pauli repulsion, electrostatic energy and orbital stabilisation [39]. The Pauli repulsion considers the exchange effects appearing between closed shell bodies of the fragments [40], not to be confused with the electrostatic repeal of the electron clouds. The electrostatic term considers the classical Coulomb part between the nuclei and clouds of the introduced fragments, at their initial superposed density distribution. The orbital term accounts all the relaxation of densities from the fragments to the final molecular consistency.

In the simplest way, the fragments can be the neutral atoms, but it is interesting to prepare in preamble the Gd^{3+} and $C_{80}{}^{6-}$ units, using for the cage the optimised geometry of the $Gd_2@C_{80}$ complex. The artificial dimer moiety $(Gd_2)^{6+}$ from the Gd^{3+} ions is unstable, as expected, with positive bonding energy, 0.4906 Hartree. The electrostatic part, 1.2390 Hartree, is very close to the point charge estimation, considering the 3.844 Å inter-nuclear distance. The Pauli repulsion is very small, about 0.0002 Hartree, in accordance to the point that lanthanides are bodies with electron density well confined around the nuclei, with small propensity for long-range interactions, except the ionic effects. However, surprisingly, the orbital stabilisation is sizeable, about −0.7486 Hartree. The situation is apparently puzzling, especially considering that the orbital scheme corresponds to a non-bonding balance, $[Xe]_2(\sigma_f)^{\alpha}(\sigma_f{}^*)^{\alpha}(\pi_f)^{2\alpha}\ (\pi_f{}^*)^{2\alpha}(\delta_f)^{2\alpha}(\delta_f{}^*)^{2\alpha}(\varphi_f)^{2\alpha}(\varphi_f{}^*)^{2\alpha}$, having both the bonding and antibonding sets occupied. The orbital stabilisation can be assigned merely to polarisation effects located on the fragment, rather than to the direct overlap of the f-type orbitals. As discussed in previous sections, the atom in dimer or in the whole molecule undergoes a deformation based on f–d slight mixing, that brings a certain stabilisation. Each orbital from the fourteen functions included in the previously ascribed configuration brings an amount of −0.05 Hartree. This uniformity, irrespective of the $\lambda = \sigma, \pi, \delta, \varphi$ axial symmetry contributors, suggests that the recorded stabilisation is not driven by the nature of the overlap.

The $Gd_2@C_{80}$ formed from two Gd^{3+} fragments and the $C_{80}{}^{6-}$ negative cage shows a net bonding stabilisation of −4.7976 Hartree. The Pauli repulsion is 0.4627 Hartree, entirely coming from the interference of lanthanide ionic bodies with the inner walls of the cluster, once previously showed that the dimer had this component almost negligible. The electrostatic term is −2.1559 Hartree, proving that the proximity of the fullerene atoms (first environment of Gd–C contacts with about 2.5 Å distances) carrying approximately evenly distributed negative charge counterbalances the mutual repeal of the lanthanide ions. The net orbital stabilisation, −3.1043 Hartree, is due also to the weak covalence established with the fullerene, by each lanthanide ion. We discard the issue of other structures resulted from the rotation of the Gd–Gd line inside the cage, since their conceivable variety can make the subject of a separate study.

Another numeric experiment follows the EDA in the hypothetical mono-lanthanide system $(Gd^{3+})@(C_{80}{}^{3-})$ when the encapsulated ion moves along the axis traced in the

dimer, from the centre of the molecule, to one side. This is a conventional system, meant to detect the bonding capabilities of a single ion against the fullerene cage, using the frozen optimal geometry of the computed $Gd_2@C_{80}$. The triply negatively charged fullerene was produced using the ADF capability to impose fractional occupation numbers, which is important in keeping the charge uniformity on the atoms of the cluster. Then, given the quadruple quasi-degenerate nature of the last occupied orbital sequence of the C_{80}, the occupation numbers were imposed in $C_{80}{}^{3-}$ as 5/8 fractional value, in each of the functions originating from the g_g set in icosahedral symmetry. The triply charged anion, instead of six negative charge of the fullerene in $Gd_2@C_{80}$, conventionally rescales the amount of interaction, when the hypothetical $Gd@C_{80}$ is taken. The results are shown in Table 2. The Pauli term has a small value when the ion is kept in centre or moved towards the side with distances up to about 1 Å. At larger off centre position, the Pauli repulsion grows exponentially, deciding the formation of the minimum before entering in the fullerene wall, as the other stabilising term continues to decrease their values along this shift.

The minimum in the total bonding energy is reached at about $dh = 1.8$ Å (in comparison to about the $dh = \pm 1.9$ Å in the case of $Gd_2@C_{80}$). The proximity of fullerene wall determines a certain covalence component, illustrated by the orbital term from Table 2. The main bonding effect can be interpreted as due to donation from the negative charge of the cage towards the empty 5d and 6s virtuals of the lanthanide ions. This conclusion is drawn examining population analysis results and is also sustained by the modelling from the following section. The electrostatic term varies a little, for the reason of a certain resemblance of the fullerene to an uniformly charged sphere, which keeps the inside potential constant. Of course, because of atomic details on the surface of the cluster, the sphere approximation does not completely hold.

Table 2. The energy decomposition analysis of the $(Gd^{3+})@(C_{80}{}^{3-})$ system when the lanthanide ion is moved from the centre ($dh = 0$) towards one margin along the Gd–Gd virtual axis. All the energy amounts are in Hartree.

dh (Å)	Pauli repulsion	Electrostatic energy	Orbital component	Total bonding
0	0.0075	−0.7524	−1.1019	−1.8468
0.25	0.0087	−0.7526	−1.1102	−1.8541
0.5	0.0102	−0.7529	−1.1203	−1.8631
0.75	0.0148	−0.7538	−1.1362	−1.8752
1	0.0257	−0.7560	−1.1619	−1.8922
1.25	0.0464	−0.7602	−1.1985	−1.9124
1.5	0.0929	−0.7705	−1.2559	−1.9335
1.75	0.1914	−0.7940	−1.3398	−1.9423
2	0.3926	−0.8452	−1.4617	−1.9143
2.25	0.6844	−0.9233	−1.5998	−1.8385

3.4. Idealisation of lanthanide-fullerene interaction as atom-in-sphere model. The Xatom+Xsphere algorithm

The series of computation modelling will be completed designing the DFT account of lanthanide atom inside a sphere. More precisely, the sphere will be considered as an uniform $Z_\Phi = 80$ positive charge, at radius $Z_\Phi = 4.12$ Å (the average radius of C_{80} fullerene), retaining a number of 83 electrons. This is a heuristic approximation of the $C_{80}{}^{3-}$ negative cluster. The sphere (labelled Φ) is treated separately or containing, in centre, a $Z_{Ln} = 64$ nucleus of Gd(III) (labelled Gd@Φ). The problem resembles the radial atomic equation, except that the central potential is enhanced by the supplementary account of the positive sphere crust. Namely, for a radial point placed inside the sphere, the potential due to the positive crust is constant, $U_\Phi(r < R_\Phi) = -Z_\Phi/R_\Phi$, while going outside, $r > R_\Phi$, it turns into a point like form: $U_\Phi(r > R_\Phi) = -Z_\Phi/r$. The potential due to the lanthanide is always central: $U_{Ln}(r) = -Z_{Ln}/r$.

The Gd@Φ ensemble is obviously described by the corresponding sum, $U_{Gd@\Phi}(r) = U_{Ln}(r) + U_\Phi(r)$. The problem is completed, in each case (the separate Gd and Φ pieces or their ensemble), with the potential due to electrostatics of charge distribution and the exchange functional part: $V(r) = U(r) + V_{Coul}(\rho(r)) + V_{xc}(\rho(r))$. As exchange functional, we simply considered the local density approximation (LDA) which is conceptually sufficient in the account of the idealised problem. The dependence on the total density $\rho(r)$ is resolved iteratively. The equation retains its spherical nature, being solved for the $V_{Ln}(r)$ and $V_\Phi(r)$ separately or for the $V_{Gd@\Phi}(r)$ composite. As function of the general radial potential $V(r)$ the radial equation is:

$$-\frac{1}{2}\left[\frac{\partial^2(rR(r))}{\partial r^2} - \frac{l(l+1)}{r^2}(rR(r))\right] + V(r)(rR) = E(rR(r)), \tag{15}$$

where $R(r)$ is the radial function and l the quantum number controlling the kinetic moment.

One of the authors has developed previously a very efficient numerical scheme [41,42] for solving this equation, by a grid method that replaces the need for a basis set. The clue is the handling of the differential operator from the above equation by a finite difference that leads to a system with tridiagonal matrices, having the lines defined as follows:

$$\left(\frac{-1}{(r_{k+1}-r_{k-1})(r_k-r_{k-1})}, \frac{1}{(r_{k+1}-r_k)(r_k-r_{k-1})} + V(r_k) + \frac{1}{2}\frac{l(l+1)}{r_k^2}, \frac{-1}{(r_{k+1}-r_{k-1})(r_{k+1}-r_k)}\right) \cdot \begin{pmatrix} r_{k-1}R_{k-1} \\ r_kR_k \\ r_{k+1}R_{k+1} \end{pmatrix} = E_l \cdot (r_kR_k). \tag{16}$$

This can be formulated as an eigenvalues–eigenvectors problem, leading directly to the radial dependence for a set of eigenfunctions, the vector set having the same dimensionality as the number of defined grid points. In spite its simplicity, the method is very powerful.

It is not the case to detail here, but it can be verified that the quasi-totality of commonly used basis sets, including those acknowledged as rich, show questionable long-range dependence. It can be tested on the simple hydrogen atom problem, observing, for instance, a very bad radial shape of 3s function for many bases (e.g. 6-311G*, cc-pv*n*Z), as compared to the known analytic solution. One may consider that a higher function as 3s will not be important in quantum chemical practice, but we take this issue as illustrative counterpoint to the presented method. The sketched numeric scheme yields, with a moderate computation cost (e.g. 100 grid points), almost perfect radial shapes for a large number of radial functions (e.g. up to 7s), keeping their quality at long-range radii. Thus, the numeric scheme is perfectly validated in a problem like the hydrogen atom, the many-electron atoms being treated in the frame of LDA, by a code popularised previously as Xatom [41]. The same scheme can be simply adapted, as we did here, for other spherical potentials, like the charged sphere or associations of point charge and sphere, the model being provisionally called Xatom + Xsphere.

Figure 5 shows an analysis of total density pattern. The Ln@Φ complex has the total density almost the sum of the Gd^{3+} and Φ fragments, a slight build up of density being visible in the panel (a) at distances between the outskirts of central ion and the wall of the sphere (the peak around 4Å). The difference density in panel (b) shows variations that can be interpreted as follows: (1) the withdraw of density from outside and surface of the sphere towards its inner part (see the depletion of $r > 4$ Å against the accumulation immediately below 4 Å); (2) at smaller extent, a part of the inner density of the lanthanide core is reinvested towards its outer region; (3) a donation from the electron population of the cage towards the lanthanide ion (in principle using its virtual orbitals as acceptors) determining the density built up in the vicinity of the $r \sim 2$ Å middle point.

For further insight, Figure 6 shows the detailed analysis on orbital components with s, p, d and f symmetries. The series of panels show that the last occupied orbitals in each set ($5s_{Gd}$, $5p_{Gd}$, $4d_{Gd}$, $4f_{Gd}$), represented by continuous line, are practically superposable on the points representing a corresponding wavefunction in the Gd@Φ complex ($5s_{Gd}$, $5p_{Gd@\Phi}$, $4d_{Gd@\Phi}$, $4f_{Gd@\Phi}$). The first virtuals of the lanthanide ion ($6s_{Gd}$, $6p_{Gd}$, $5d_{Gd}$, $5f_{Gd}$) are shown with light tone line. The Gd@Φ assembly shows the built of series of functions occupied with electrons formally originating from the cage, having the appearance of hybrids between the function on the empty sphere and the corresponding lanthanide virtuals. This trend is most visible for the d case (see the $D_{Gd@\Phi}$ profile showing maxima parallel to both $5d_{Gd}$ and D_Φ lines), sustaining the above statements about the role of 5d orbitals in the bonding scheme of the lanthanide complexes. In turn, the f orbitals show almost no trace of such a deformation effect, the $F_{Gd@\Phi}$ dotted profile being coincident to F_Φ, with no hybridisation to $5f_{Gd}$. This result is consistent with the above considerations on the f-shell rigidity against changes from outer perturbations.

The changes in P set are relatively small, while for the S orbitals the displacements at the complex formation are intermediate between those recorded for the S and D cases. This suggests, in line with the observations noted in the LF section, that the 6s component is the next in line, after 5d virtuals in providing binding effects, being acceptor for electron density provided by the environment. The outlined simple model provides clear information, in the frame of considered idealisation, about the bonding capabilities of lanthanide ions.

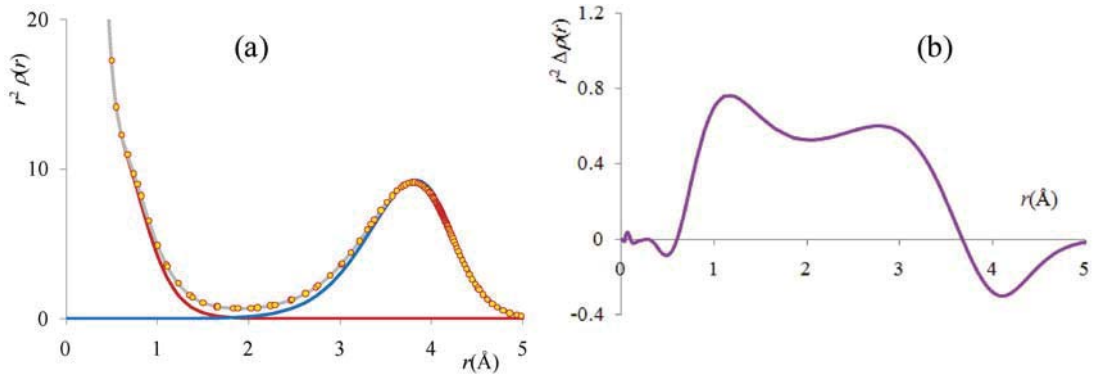

Figure 5. The Xatom + Xsphere modelling of density pattern for the Gd^{3+} lanthanide ion placed in a sphere carrying 86 electrons on a surface charged with $Z_\Phi = 80$, mimicking the spherical smearing of the $C_{80}{}^{3-}$ cluster. The panel (a) shows the density from separate calculation on lanthanide (left-hand side continuous line) and sphere (right-hand side line), the individual curves being almost superposed with the ensemble density, figured with line and points. The panel (b) shows the density difference between complex and its components.

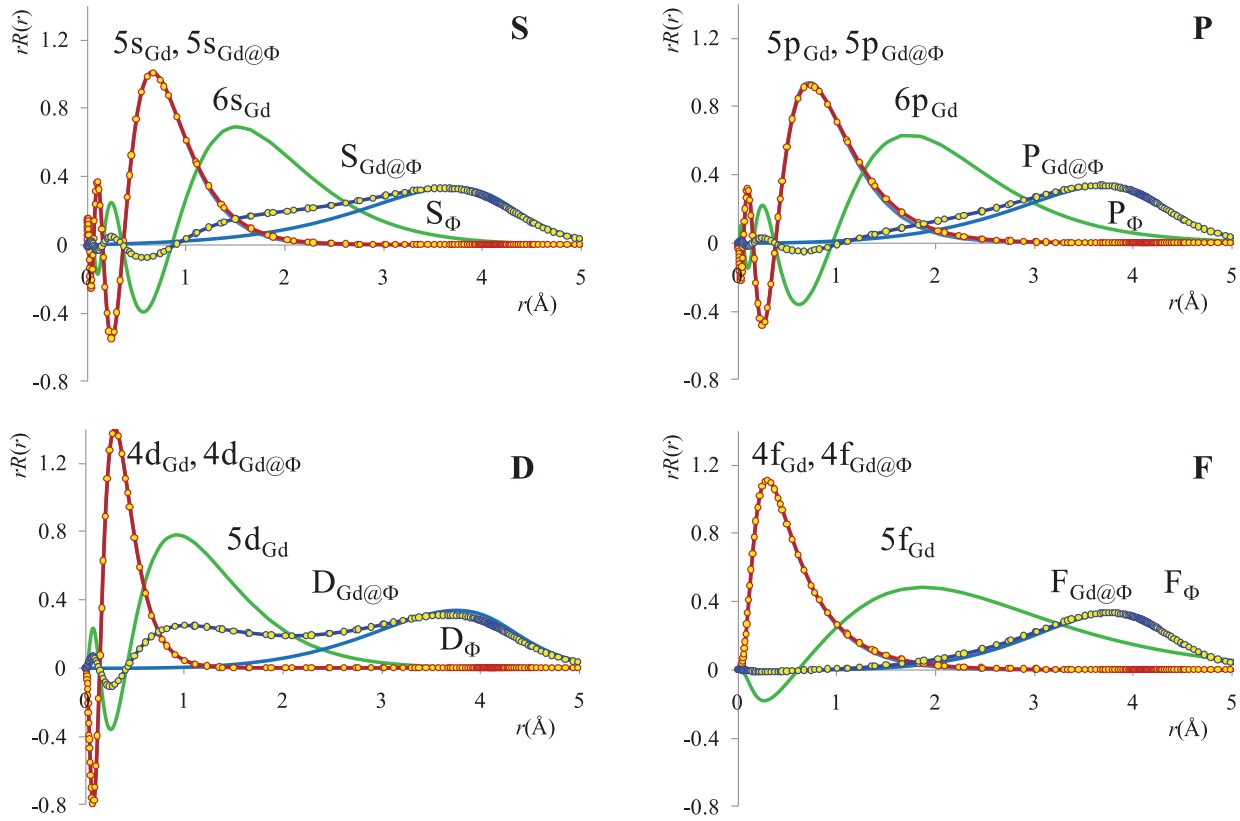

Figure 6. The orbital details of the Xatom+Xsphere, dichotomised on the S, P, D and F spherical symmetries. The calculations shows the components of separate ion (Gd^{3+}) or sphere (Φ) calculations (continuous curves) and the related profiles in the Gd@Φ ensemble (marked with points).

4. Conclusion

Using a palette of different computational methods and interpretations based on model Hamiltonians, we analysed the particularities of bonding regime for lanthanide ions embedded in fullerenes. For the $Gd_2@C_{80}$ and $Gd_2@C_{79}N$ compared examples, the exchange coupling was discussed, the last system being experimentally evidenced with a ferromagnetic ground state [18]. The specific difference is that in the C_{80} case the hexa-anionic cage is diamagnetic, while the analogous heterofullerene anion carries an unpaired spin. The calculations show that, in fact, the fullerene spin component is transferred on functions originating from the 5d virtuals of lanthanide ions, this factor determining the overall ferromagnetic appearance. The intra-atomic 4f–5d parallel spin coupling determines a ferromagnetic alignment of the f-shell spins to the electron placed on the upper orbit of the $(Gd_2)^{5+}$ trapped dimer moiety. Both the multi-configuration CASSCF calculation and the BS-DFT approach showed a strong coupling parameter, of about 400 cm^{-1}, for the $Gd_2@C_{79}N$ system.

The situation of a lanthanide centre, interacting, at one side with a hexagonal face of the fullerene cluster and, at other side with the positive charge of its companion in dimer, is described with an extended version of LF modelling, based on FDE DFT calculations. The current versions of LF methods, dedicated to f or d shells suffer from a tacit drawback, the holohedrisation effect, marking the incapacity to account correctly the asymmetric environments. The multi-shell LF developed recently by us [36] is applied here for the description of the highly polar environment felt by a lanthanide ion.

The discussion of bonding features was continued with EDA, performing the dichotomy in Pauli repulsion, electrostatic part and orbital stabilisation contributions.

The situation of the encapsulated lanthanide ion was further considered in the frame of a heuristic atom-in-sphere model, using original codes, for numeric experiments following the deformation of density and orbital profiles in the sum of unperturbed entities (Gd^{3+} and a charged sphere containing it) in comparison to the interacting systems. This modelling revealed that the bonding of the lanthanide units is merely realised with the help of 5d virtuals, while the 4f shell is chemically inert, as also was pointed previously [20] and can be figured from the actual quantum chemical calculations.

Disclosure statement

No potential conflict of interest was reported by the authors.

Funding

This work is supported by the Swiss National Science Foundation; by the Swiss State Secretariat for Research and Innovation; by the UEFISCDI research grants PCE 14/2013 (Romania).

References

[1] A.A. Popov, S. Yang, and L. Dunsch, Chem. Rev. **113**, 5989 (2013).

[2] M. Rudolf, S. Wolfrum, D.M. Guldi, L. Feng, T. Tsuchiya, T. Akasaka, and L. Echegoyen, Chem. Eur. J. **18**, 5136 (2012); H.C. Dorn and P.P Fatouros, Nanosci. Nanotechnol. Lett. **2**, 65 (2010).

[3] W. Andreoni and A. Curioni, in *The Chemical Physics of Fullerenes*, edited by W. Andreoni (Kluwer, Dordrecht, 1996), pp. 183–196.

[4] F. Cimpoesu, N. Dragoe, H. Ramanantoanina, W. Urland, and C. Daul, Phys. Chem. Chem. Phys. **16**, 11337 (2014).

[5] R. Westerström, J. Dreiser, C. Piamonteze, M. Muntwiler, S. Weyeneth, H. Brune, S. Rusponi, F. Nolting, A. Popov, S. Yang, L. Dunsch, and T. Greber, J. Am. Chem. Soc. **134**, 9840 (2012).

[6] M. Ferbinteanu, F. Cimpoesu, M.A. Gîrtu, C. Enachescu, and S. Tanase, Inorg. Chem. **51**, 40 (2012); F. Cimpoesu, S. Dahan, S. Ladeira, M. Ferbinteanu, and J.-P. Costes, *ibid*. **51**, 11279 (2012).

[7] H. Ramanantoanina, W. Urland, F. Cimpoesu, and C. Daul, Phys. Chem. Chem. Phys. **15**, 13902 (2013); H. Ramanantoanina, W. Urland, A. García-Fuente, F. Cimpoesu, and C. Daul, Chem. Phys. Lett. **588**, 260 (2013); Phys. Chem. Chem. Phys. **16**, 14625 (2014).

[8] M. Zbiri, C. Daul, and T.A. Wesolowski, J. Chem. Theor. Comput. **2**, 1106 (2006); A. Borel, L. Helm, and C. Daul, Chem. Phys. Lett. **383**, 584 (2004); M. Zbiri, M. Atanasov, C. Daul, J.M. Garcia-Lastra, and T.A. Wesolowski, *ibid*. **397**, 441 (2004); M. Atanasov, C. Daul, H.U. Güdel, T.A. Wesolowski, and M. Zbiri, Inorg. Chem. **44**, 2954 (2005).

[9] M. Atanasov, C. Daul, and C. Rauzy, Chem. Phys. Lett. **367**, 737 (2003); C. Daul, Int. J. Quantum Chem. **52**, 867 (1994); T. Minerva, A. Goursot, and C. Daul, Chem. Phys. Lett. **350**, 147 (2001).

[10] J. Paulovic, F. Cimpoesu, M. Ferbinteanu, and K. Hirao, J. Am. Chem. Soc. **126**, 3321 (2004); M. Ferbinteanu, T. Kajiwara, K.-Y. Choi, H. Nojiri, A. Nakamoto, N. Kojima, F. Cimpoesu, Y. Fujimura, S. Takaishi, and M. Yamashita, J. Am. Chem. Soc. **128**, 9008 (2006).

[11] W. Urland, Chem. Phys. **14**, 393 (1976); W. Urland, Chem. Phys. Lett. **46**, 457 (1977); W. Urland, *ibid*. **77**, 58 (1981); W. Urland, *ibid*. **83**, 116 (1981).

[12] W. Urland and R. Kremer, Inorg. Chem. **23**, 1550 (1984); S.T. Hatscher and W. Urland, J. Solid State Chem. **176**, 288 (2003); F. Soetebier and W. Urland, Eur. J. Inorg. Chem. **7**, 1673 (2002).

[13] E.G. Gillan, C. Yeretzian, K.S. Min, M.M. Alvarez, R.L. Whetten, and R.B. Kaner, J. Phys. Chem. **96**, 6869 (1992); J. Ding and S. Yang, Angew. Chem., Int. Ed. Engl. **35**, 2234 (1996).

[14] T. Suzuki, Y. Maruyama, T. Kato, K. Kikuchi, Y Nakao, Y. Achiba, K. Kobayashi, and S. Nagase, Angew. Chem. **107**, 1228 (1995); Angew. Chem., Int. Ed. Engl. **34**, 1094 (1995).

[15] K. Kobayashi, S. Nagase, and T. Akasaka, Chem. Phys. Lett. **245**, 230 (1995).

[16] B P. Cao, T. Wakahara, T. Tsuchiya, M. Kondo, Y. Maeda, G.M.A. Rahman, T. Akasaka, K. Kobayashi, S. Nagase, and K. Yamamoto, J. Am. Chem. Soc. **126**, 9164 (2004); B. Cao, H. Nikawa, T. Nakahodo, T. Tsuchiya, Y. Maeda, T. Akasaka, H. Sawa, Z. Slanina, N. Mizorogi, and S. Nagase, *ibid*. **130**, 983 (2008); M. Yamada, T. Wakahara, T. Tsuchiya, Y. Maeda, M. Kako, T. Akasaka, K. Yoza, E. Horn, N. Mizorogi, and S. Nagase, Chem. Commun. **5**, 558 (2008).

[17] M.M. Olmstead, A. de Bettencourt-Dias, S. Stevenson, H.C. Dorn, and A.L. Balch, J. Am. Chem. Soc. **124**, 4172 (2002); Y. Ito, T. Okazaki, S. Okubo, M. Akachi, Y. Ohno, T. Mizutani, T. Nakamura, R. Kitaura, T. Sugai, and H. Shinohara, ACS Nano **1**, 456 (2007); K. Kikuchi, K. Akiyama, K. Sakaguchi, T. Kodama, H. Nishikawa, I. Ikemoto, T. Ishigaki, Y. Achiba, K. Sueki, and H. Nakahara, Chem. Phys. Lett. **319**, 472 (2000).

[18] W. Fu, J. Zhang, T. Fuhrer, H. Champion, K. Furukawa, T. Kato, J.E. Mahaney, B.G. Burke, K.A. Williams, K. Walker, C. Dixon, J. Ge, C. Shu, K. Harich, and H.C. Dorn, J. Am. Chem. Soc. **133**, 9741 (2011).

[19] O. Kahn, Struct. Bonding **68**, 89 (1987); O. Guillou, R.L. Oushoorn, O. Kahn, K. Boubekeur, and P. Batail, Angew. Chem., Int. Ed. Engl. **31**, 626 (1992); C. Benelli, A. Caneschi, D. Gatteschi, O. Guillou, and L. Pardi, Inorg. Chem. **29**, 1750 (1990).

[20] M. Ferbinteanu, A. Zaharia, M.A. Gîrţu, and F. Cimpoesu, Cent. Eur. J. Chem. **8**, 519 (2010); M. Ferbinteanu, F. Cimpoesu, and S. Tanase, Struct. Bond. **163**, 185 (2015).

[21] A.A. Popov, J. Comput. Theor. Nanosci. **6**, 292 (2009); A. A. Popov, L. Zhang, and L. Dunsch, ACS Nano. **4**, 795 (2010); H. Umemoto, K. Ohashi, T. Inoue, N. Fukui, T. Sugai, and H. Shinohara, Chem. Commun. **46**, 5653, (2010).

[22] H. Kurihara, X. Lu, Y. Iiduka, N. Mizorogi, Z. Slanina, T. Tsuchiya, S. Nagase, and T. Akasaka, Chem. Commun. **48**, 1290 (2012); T. Yang, X. Zhao, and E. Osawa, Chem. Eur. J. **7**, 10230 (2011); A.A. Popov and L. Dunsch, J. Am. Chem. Soc. **130**, 17726 (2008).

[23] H. Zheng, X. Zhao, W.-W. Wang, T. Yang, and S. Nagase, J. Chem. Phys. **137**, 014308 (2012); Y. Iiduka, O. Ikenaga, A. Sakuraba, T. Wakahara, T. Tsuchiya, Y. Maeda, T. Nakahodo, T. Akasaka, M. Kako, N. Mizorogi, and S. Nagase, J. Am. Chem. Soc. **127**, 9956 (2005).

[24] K. Furukawa, S. Okubo, H. Kato, H. Shinohara and T. Kato, J. Phys. Chem. A **107**, 10933 (2003)

[25] M.W. Schmidt, K.K. Baldridge, J.A. Boatz, S.T. Elbert, M.S. Gordon, J.H. Jensen, S. Koseki, N. Matsunaga, K.A. Nguyen, S.J. Su, T.L. Windus, M. Dupuis, and J.A. Montgomery, J. Comput. Chem. **14**, 1347 (1993).

[26] W.J. Stevens, H. Basch, and M. Krauss, J. Chem. Phys. **81**, 6026 (1984); W.J. Stevens, M. Krauss, H. Basch, and P.G. Jasien, Can. J. Chem. **70**, 612 (1992); T.R. Cundari and W.J. Stevens, J. Chem. Phys. **98**, 5555 (1993).

[27] F. Neese, *ORCA – an ab initio, Density Functional and Semiempirical Program Package* (Max-Planck Institute for Energie Conversion, Mülheim an der Ruhr, Germany, 2013).

[28] ADF2012.01, SCM, Theoretical Chemistry, Vrije Universiteit, Amsterdam, (2012). <http://www.scm.com>;

G. te Velde, F.M. Bickelhaupt, S.J.A. van Gisbergen, C. Fonseca Guerra, E.J. Baerends, J.G. Snijders, and T. Ziegler, J. Comput. Chem. **22**, 931 (2001); C. Fonseca Guerra, J.G. Snijders, G. te Velde, and E.J. Baerends, Theor. Chem. Acc. **99**, 391 (1998).

[29] A.D. Becke, Phys. Rev. A **38**, 3098 (1988); J.P. Perdew, Phys. Rev. B **33**, 8822 (1986).

[30] G. Yaglioglu, R. Pino, R. Dorsinville, and J.Z. Liu, Appl. Phys. Lett. **78**, 898. (2001)

[31] L. Noodleman and J.G. Norman, J. Chem. Phys. **70**, 4903 (1979); L. Noodleman, J. Chem. Phys. **74**, 5737 (1981); A. Bencini and F. Totti, Int. J. Quantum Chem. **101**, 819 (2005); M. Mitani, V. Mori, Y. Takano, D. Yamaki, Y. Yoshioka, and K. Yamaguchi, Chem. Phys. **113**, 4035 (2000).

[32] T.A. Wesolowski and A. Warshel, J. Phys. Chem. **97**, 8050 (1993); J. Neugebauer, C.R. Jacob, T.A. Wesolowski, and E.J. Baerends, J. Phys. Chem. A **109**, 7805 (2005).

[33] B.N. Figgis and M.A. Hitchman, *Ligand Field Theory and its Applications* (Wiley-VCH, New York, 2000); E.I. Solomon and A.B.P. Lever, editors, *Inorganic Electronic Structure and Spectroscopy* (Wiley & Sons, New York, 1999).

[34] S Hüfner, *Optical Spectra of Transparent Rare Earth Compounds* (Academic Press, New York, 1978); D.J. Newman and B. Ng, *Crystal Field Handbook* (Cambridge University Press, Cambridge, 2000).

[35] C.F. Schäffer, Proc. R. Soc. A **297**, 96 (1967); C.F. Schäffer, Theor. Chim. Acta **4**, 166 (1966).

[36] H. Ramanantoanina, W. Urland, F. Cimpoesu, and C. Daul, Phys. Chem. Chem. Phys. **16**, 12282 (2014).

[37] E.K.U. Gross, L.N. Oliveria, and W. Kohn, Phys. Rev. A **37**, 2809 (1988); C.A. Ullrich and W. Kohn, Phys. Rev. Lett. **87**, 093001 (2001); E. Cances, J. Chem. Phys. **114**, 10616 (2001).

[38] T. Ziegler and A. Rauk, Theor. Chim. Acta **46**, 1 (1977); M. von Hopffgarten and G. Frenking, WIREs Comput. Mol. Sci. **2**, 43 (2012).

[39] C.E. Dykstra, G. Frenking, K.S. Kim, and G.E. Scuseria, *Theory and Applications of Computational Chemistry* (Elsevier B.V., Amsterdam, 2005), p. 291.

[40] O.V. Gritsenko, P.R.T. Schipper, and E.J. Baerends, Phys. Rev. A **57**, 3450 (1998).

[41] C.A. Daul, Xatom. <http://www.chem.unifr.ch/cd/download/files/Xatom_lite.zip>.

[42] A. Borel, L. Helm, and C.A. Daul, Chem. Phys. Lett. **383**, 584 (2004).